Supplementary Information

Hydrogen Sorption on Microporous Carbon/Sulfur Nanocomposites Systems

Charles D. Brewster,[a] *Lui R. Terry,*[b] *Huan V. Doan,*[b] *Sebastien Rochat,*[c] *Valeska P. Ting,*[b,d,e*]

[a] Bristol Composites Institute, Department of Aerospace Engineering, University of Bristol, Bristol, BS8 1TR, U.K

[b] Bristol Composites Institute, Department of Mechanical Engineering, University of Bristol, Bristol, BS8 1TR, U.K

[c] Bristol Composites Institute, School of Chemistry, University of Bristol, Bristol, BS8 1TR, U.K

[d] College of Engineering, Computing and Cybernetics, Australian National University, Canberra, ACT 0200, Australia

[e] Research School of Chemistry, Australian National University, Canberra, ACT 0200, Australia

Contact Information

Charles D. Brewster: c.d.brewster@bristol.ac.uk

Lui R. Terry: lt7006@bristol.ac.uk

Huan V. Doan: huan.doan@bristol.ac.uk

Sebastien Rochat: s.rochat@bristol.ac.uk

*Corresponding Author

Valeska P. Ting: v.ting@bristol.ac.uk

H-Shaped Ampule

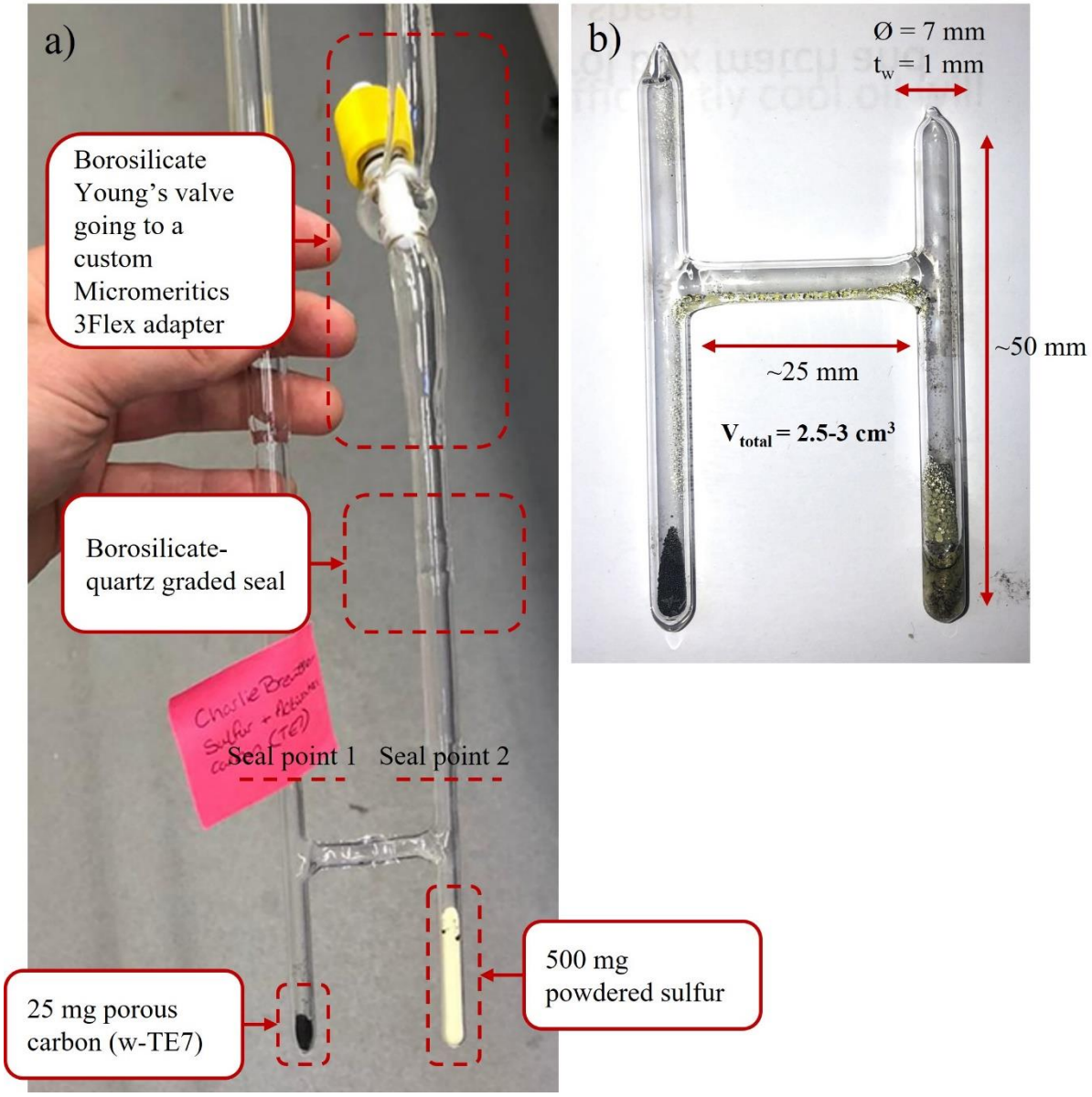

Figure S1: a) Bespoke H-shaped quartz tube used in the synthesis of the sulfur/carbon nanocomposites (w-TE7 and sulfur in this instance) prior to sealing. Labelled points show connections and adaptors to attach to instrument and maintain pressure <1 Pa and approximate seal points to achieve desired dimensions. b) Sealed H-shaped quartz ampule following heating in tube furnace showing approximate dimensions of the specimen.

Semi-Empirical Modelling of High-Pressure Hydrogen Sorption Excess Isotherms

Equation 1 within the main text was fitted to the experimental H_2 gas sorption isotherms using the Levenberg-Marquardt algorithm to identify the set of parameters that minimises the sum of squares using the Origin lab software (Origin 2020b).

In order to fit Equation 1, ρ_b must be expressed in term of $\rho_b(P,T)$, this can be acheived via the real gas equation (see Equation (SI.1)).

$$\rho_b(P,T) = \frac{1}{Z(P,T)}\frac{P \cdot M}{R \cdot T} \qquad \text{(SI.1)}$$

Where $Z(P,T)$ is the compressibility with respect to temperature and pressure, P is pressure in MPa, M is the molecular mass of H_2 equal to 2.01565×10^{-3} kg.mol^{-1}, R is the gas constant equal to 8.314×10^{-6} m^3.MPa.K^{-1}.mol^{-1} and T is temperature in K. Isothermal 77 K H_2 density data was provided by NIST Chemical WebBook [1] and converted to $Z(P,77\,K)$ via appropriate rearrangement of Equation SI.1. A rational equation (see Equation SI.2) was fitted to the $Z(P,77\,K)$ data, which provides the constants e, f , g and h allowing expression of Z soley in terms of pressure. e and f are in units MPa^{-1}. g and h are in units MPa^{-2}.

$$Z(P) = \frac{1 + e \cdot P + f \cdot P^2}{1 + g \cdot P + h \cdot P^2} \qquad \text{(SI.2)}$$

Substitution of Equation SI.2 into Equation 1 allows accurate interpolation of $\rho_b(P,77\,K)$ at any experimental pressure value.

Thermogravimetric Analysis

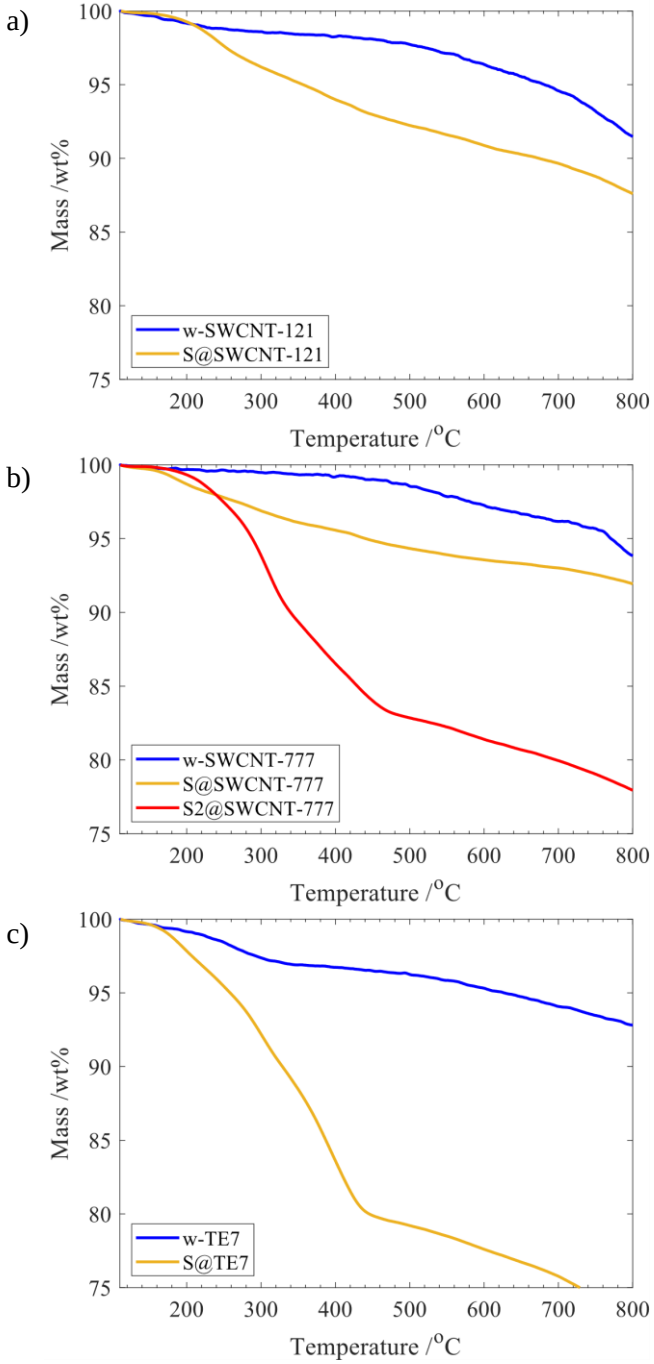

Figure S2: Thermogravimetric analysis used to determine the sulfur content of the composite material in a) w-SWCNT-121 (blue) and S@SWCNT-121 (yellow) ; b) w-SWCNT-777 (blue), S@SWCNT-777 (yellow) and S2@SWCNT-777 (red) ; c) w-TE7 (blue) and S@TE7 (yellow). All plots have been normalised to the end of the isothermal dwell at 110 °C to exclude the mass loss due to moisture, and have been smoothed using the Savizky-Golay method.

X-ray Photoelectron Spectroscopy

Table S1: Elemental composition of the washed carbon samples and sulfur-doped composite sample as determined from the X-ray Photoelectron Spectroscopy survey-spectra.

	Element	Peak	Abundance wt%
w-SWCNT-121	Carbon	C 1s	94.56
	Oxygen	O 1s	5.44
S@SWCNT-121	Carbon	C 1s	81.57
	Sulfur	S 2p	14.76
	Oxygen	O 1s	3.31
	Silicon	Si 2p	0.36
w-SWCNT-777	Carbon	C 1s	94.00
	Oxygen	O 1s	4.48
	Nitrogen	N 1s	0.81
	Silicon	Si 2p	0.72
S@SWCNT-777	Carbon	C 1s	86.06
	Sulfur	S 2p	9.32
	Oxygen	O 1s	2.94
	Molybdenum	Mo 3d5	1.67
w-TE7	Carbon	C 1s	91.22
	Oxygen	O 1s	6.58
	Silicon	Si 2p	0.83
	Nitrogen	N 1s	0.67
	Sulfur	S 2p	0.37
	Chlorine	Cl 2p	0.32
S@TE7	Carbon	C 1s	81.02
	Sulfur	S 2p	14.46
	Oxygen	O 1s	3.57
	Nitrogen	N 1s	0.96

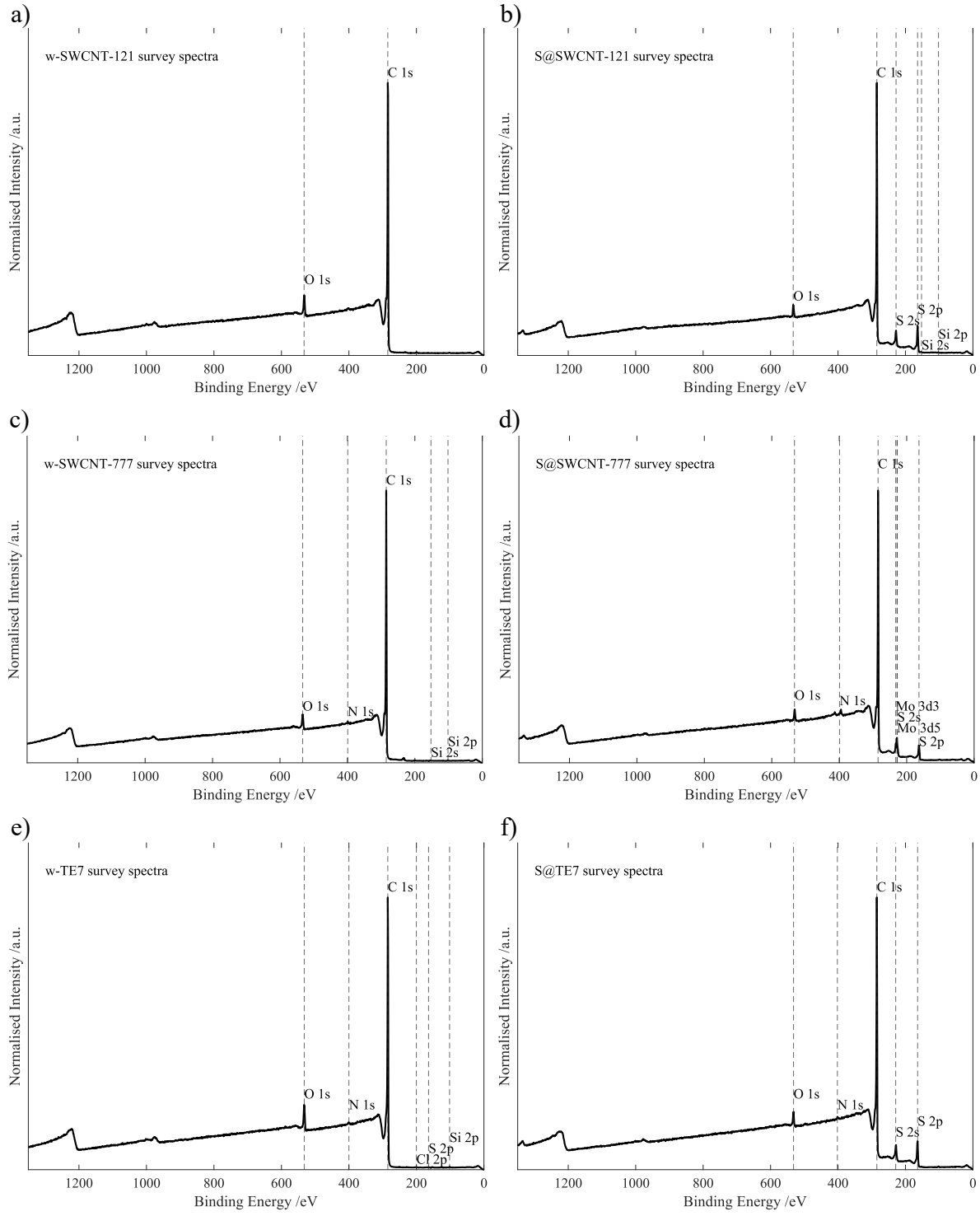

Figure S3: Normalised XPS spectra from a) w-SWCNT-121; b) S@SWCNT-121; c) w-SWCNT-777 ; d) S@SWCNT-777; e) w-TE7; and f) S@TE7. All XPS spectra show peaks determined via the Thermo Avantage enhanced survey ID. Survey scans were conducted at a pass energy of 160 eV with a filament current = 27 A, charge balance = 3.3 V and filament bias of 3.8 V. All data was collected at pressures $<1\times10^{-8}$ Torr .

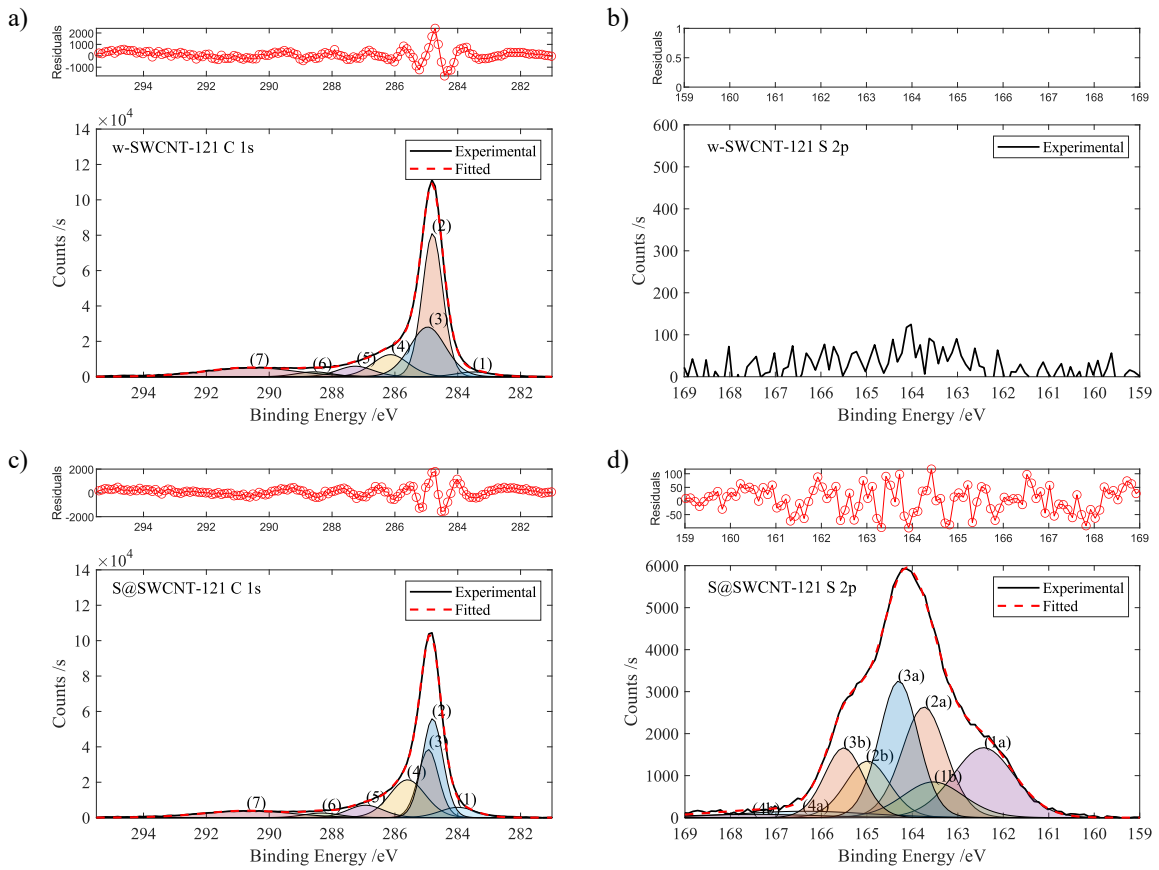

Figure S4: XPS Peak fitting results and the residuals of the fitting for: a) the C 1s spectra for w-SWCNT-12; b) the S 2p spectra for w-SWCNT-121 ; c) the C 1s spectra for S@SWCNT-121 and d) the S 2p spectra for S@SWCNT-121. For a summary of peak allocations, see Table S2. High-resolution scans were conducted at a pass energy of 20 eV with a filament current = 27 A, charge balance = 3.3 V and filament bias of 3.8 V. All data was collected at pressures <1×10^{-8} Torr.

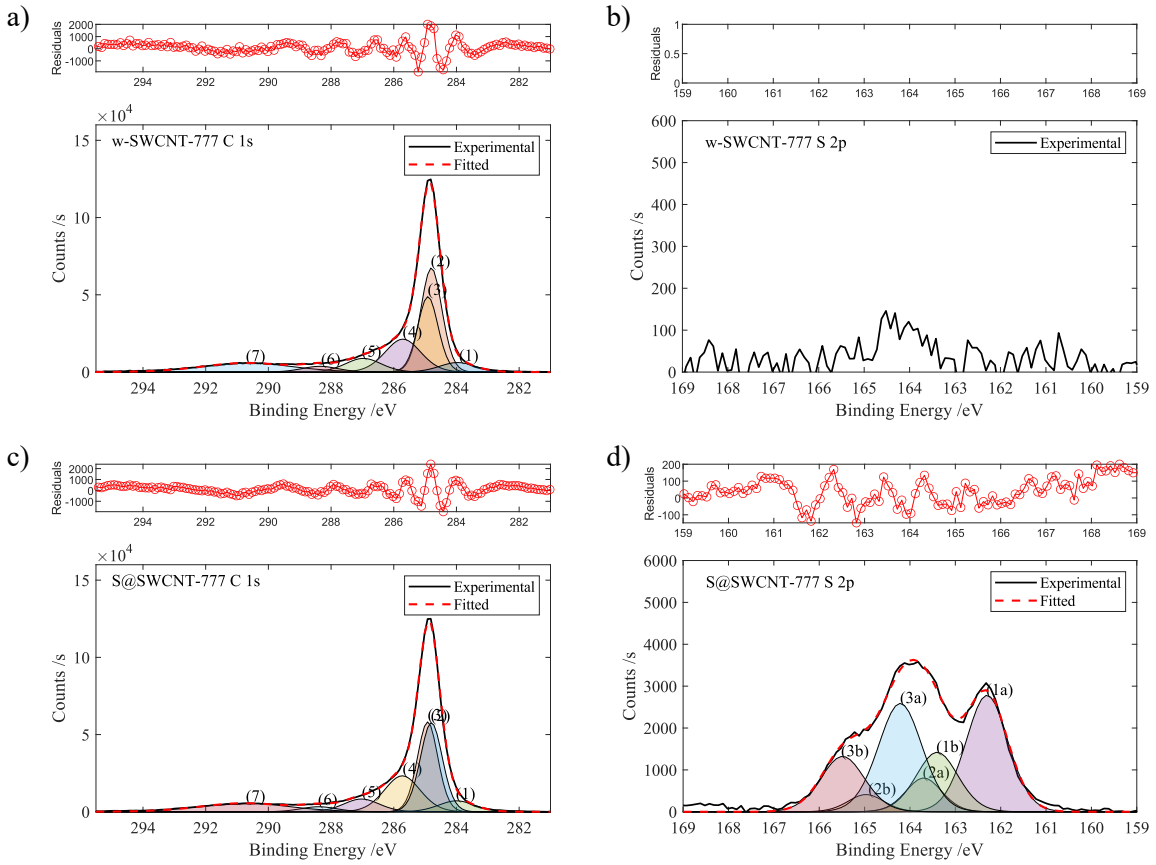

Figure S5: a) Peak fitting results of the C 1s spectra for w-SWCNT-777 and the residuals of the fitting. b) Peak fitting results of the S 2p spectra for w-SWCNT-777 and the residuals of the fitting. c) Peak fitting results of the C 1s spectra for S@SWCNT-777 and the residuals of the fitting. d) Peak fitting results of the S 2p spectra for S@SWCNT-777 and the residuals of the fitting. For a summary of peak allocations, see Table S2. High-resolution scans were conducted at a pass energy of 20 eV with a filament current = 27 A, charge balance = 3.3 V and filament bias of 3.8 V. All data was collected at pressures <1×10^{-8} Torr.

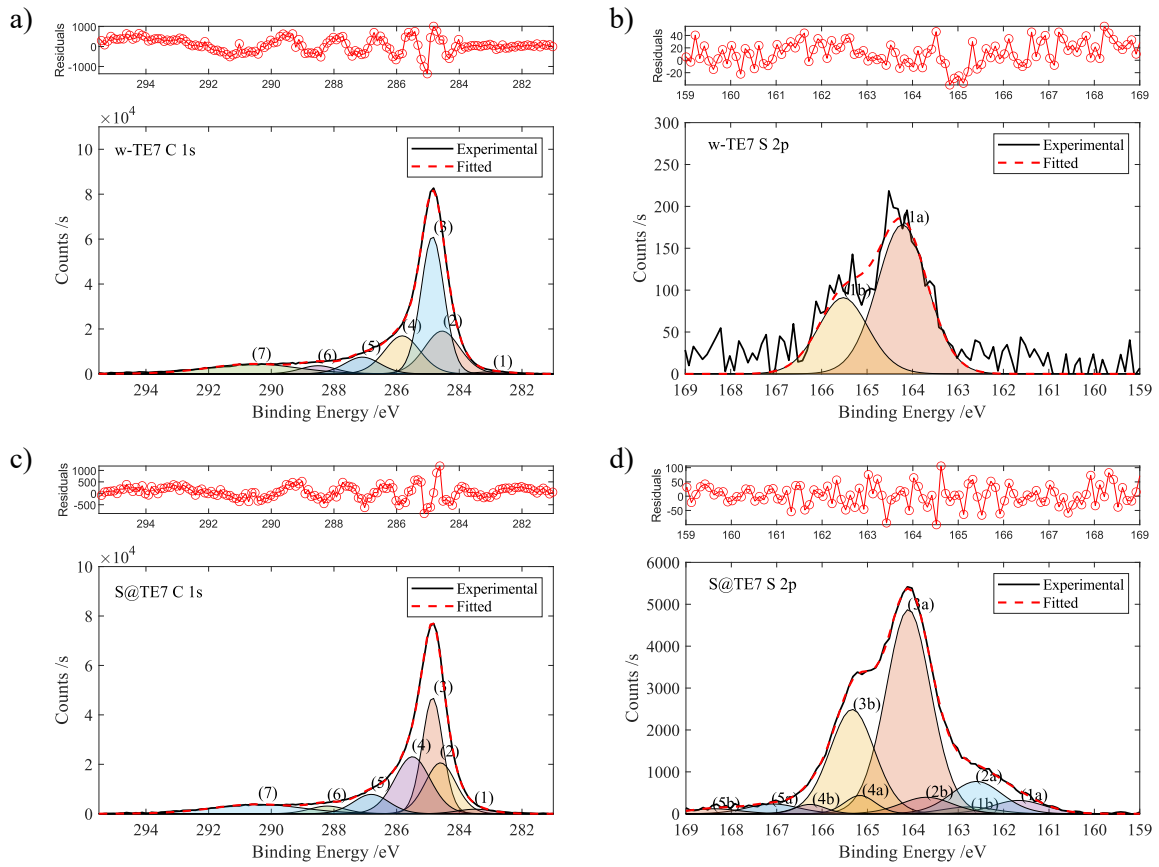

Figure S6: XPS Peak fitting results and the residuals of the fitting for a) the C 1s spectra for w-TE7; b) the S 2p spectra for w-TE7 ; c) the C 1s spectra for S@TE7 ; d) the S 2p spectra for S@TE7. For a summary of peak allocations, see Table S2. High-resolution scans were conducted at a pass energy of 20 eV with a filament current = 27 A, charge balance = 3.3 V and filament bias of 3.8 V. All data was collected at pressures <1×10^{-8} Torr .

Table S2: Summary of the literature and database searches for the peaks determined in fitting of the C 1s and S 2p peaks of each sample.

Sample	Peak	Label	Peak Position /eV	Chemical Species
w-SWCNT-121	C 1s	(1)	283.48	metal carbide[2]
		(2)	284.80	sp^2 (C=C) [2]
		(3)	284.96	sp^3 (C-C) [2]
		(4)	286.14	C-O[2]
		(5)	287.26	C=O[2]
		(6)	288.57	O-C=O[2]
		(7)	290.60	π- π^*[2]
	S 2p	~	~	~
S@SWCNT-121	C 1s	(1)	284.00	metal carbide[2]
		(2)	284.80	sp^2 (C=C) [2]
		(3)	284.93	sp^3 (C-C) [2]
		(4)	285.60	C-O[2]
		(5)	286.93	C=O[2]
		(6)	288.33	O-C=O[2]
		(7)	290.70	π- π^*[2]
	S 2p	(1a)/(1b)	162.44/163.54	C-S-H (thiol)[3], polysulfide (terminal) [4, 5], various metal sulfide [6, 7]
		(2a)/(2b)	163.74/164.98	C-S-C[3, 6, 8, 9], thiophene[3, 10], $S_{x\ (2<x<8)}$[3], polysulfide (central) [4, 11]
		(3a)/(3b)	164.30/165.51	C-S-H[6], polysulfide[12], S_8[13], thiophene[3, 7]
		(4a)/(4b)	166.37/167.47	S-O, S=O[3], $Na_2(SO_3)_2$[6]
w-SWCNT-777	C 1s	(1)	283.97	metal carbide[2]
		(2)	284.80	sp^2 (C=C) [2]
		(3)	284.91	sp^3 (C-C) [2]
		(4)	285.71	C-O[2]
		(5)	286.97	C=O[2]
		(6)	288.36	O-C=O[2]
		(7)	290.68	π- π^*[2]
	S 2p	~	~	~
S@SWCNT-777	C 1s	(1)	284.00	metal carbide[2]
		(2)	284.80	sp^2 (C=C) [2]
		(3)	284.92	sp^3 (C-C) [2]
		(4)	285.73	C-O[2]
		(5)	287.03	C=O[2]
		(6)	288.40	O-C=O[2]
		(7)	290.76	π- π^*[2]
	S 2p	(1a)/(1b)	162.30/163.40	C-S-H (thiol)[3], polysulfide (terminal) [4, 5], various metal sulfide [6, 7]
		(2a)/(2b)	163.70/164.97	C-S-C[3, 6, 8, 9], thiophene[3, 10], $S_{x\ (2<x<8)}$ [3, 14], polysulfide (central)[4, 11]
		(3a)/(3b)	164.21/165.48	C-S-H[6], polysulfide[12], S_8[13], thiophene[3, 7]
w-TE7	C 1s	(1)	282.89	metal carbide[2]
		(2)	284.55	sp^2 (C=C) [2]
		(3)	284.86	sp^3 (C-C) [2]
		(4)	285.82	C-O[2]
		(5)	287.09	C=O[2]
		(6)	288.51	O-C=O[2]
		(7)	290.58	π- π^*[2]
	S 2p	(1a)/(1b)	164.22/165.52	C-S-H[6], polysulfide[12], S_8[13], thiophene[3, 7],
S@TE7	C 1s	(1)	283.50	metal carbide[2]
		(2)	284.60	sp^2 (C=C) [2]
		(3)	284.85	sp^3 (C-C) [2]
		(4)	285.50	C-O[2]
		(5)	286.81	C=O[2]
		(6)	288.21	O-C=O[2]
		(7)	290.44	π- π^*[2]
	S 2p	(1a)/(1b)	161.67/162.77	various metal sulfide [6, 7]
		(2a)/(2b)	162.60/163.70	C-S-H (thiophene)[3], C-S-H (thiol) [3], various metal sulfide [6, 7]

(3a)/(3b)	164.10/165.34	C-S-H[6], -S-S- [3], S_8[3], thiophene[3, 7],
(4a)/(4b)	165.16/166.26	-S-S-[3, 15],
(5a)/(5b)	167.09/168.39	C-SO_2-C [3, 6, 7]

Summary of the X-ray photoelectron Spectroscopy (XPS) survey spectra provide insight into the elemental composition of the area investigated to a probable depth of approximately 10 nm. As expected, the primary component of each sample is carbon (C 1s). Following vapour deposition (and annealing), an increase in the S 2p peak is observed, indicating a greater concentration of sulfur within the composite materials. However, w-TE7 shows the presence of a small quantity of sulfur. Analysis of the S 2p spectra for w-TE7 reveals the sulfur is likely thiol or thiophene groups within the sample (possibly resulting from impurities in the precursor petroleum material).

Peak fitting of the C 1s spectra was achieved using fitting recommendations provided by Gengenbach *et al*. and can generally be achieved using 7 peaks limited to a full-width half maxima of 0.5-1.4 eV [16]. The prominent peak at approximately 284.8 eV shows the sp^2 and sp^3 hybridisations of carbon. Deconvolution of these peaks is challenging due to the overlap of the sp^2 and sp^3 peaks. However, after exposure to sulfur vapour and further annealing, there seemed to be a decrease in the relative peak area associated with sp^2 carbon, for both SWCNT samples, implying slight changes in the carbon structure due to the incorporation of sulfur, as supported by Raman Spectroscopy within the main text. Higher binding energy peaks indicate bonding to more electronegative elements such as oxygen. Owing to the relatively high abundance of oxygen in all survey spectra, the peaks at ~285.5, ~286.9 and ~288.4 eV are attributed to hydroxyl, aldehyde/ketone, and carboxyl groups, respectively. Additionally, all spectra display a weak peak below 284 eV, which implies the presence of a small quantity of metal carbide.

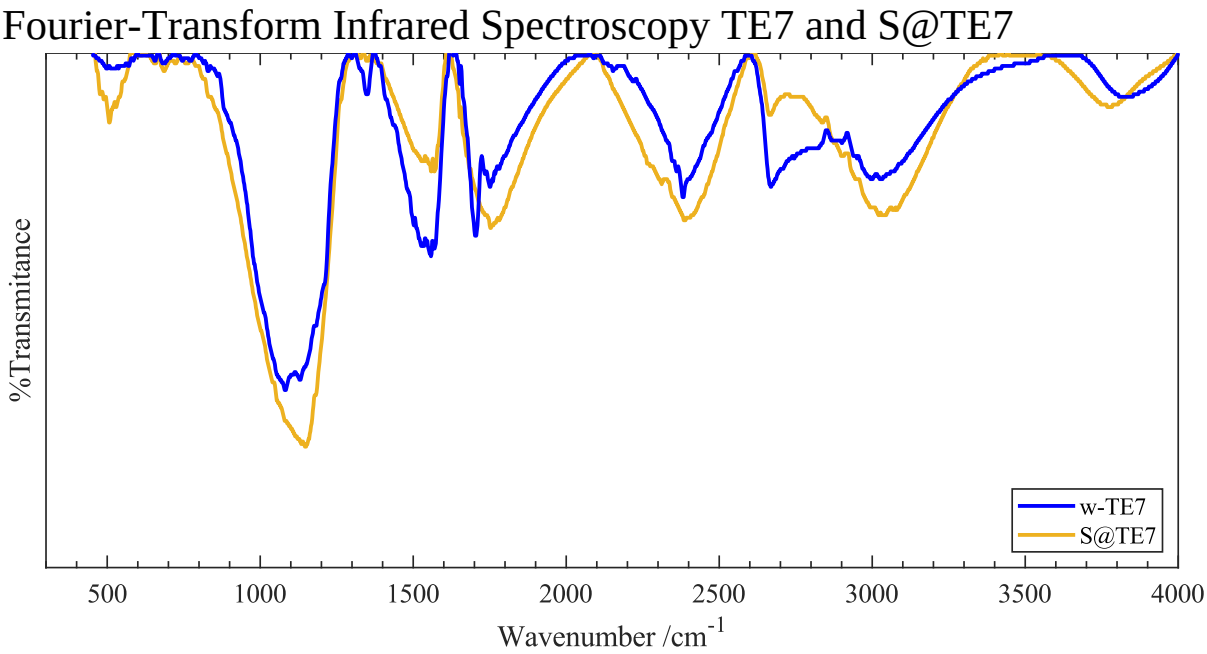

Figure S7: Fourier Transform Infrared Spectroscopy spectra of w-TE7 (blue) and S@TE7 providing evidence of an oxidation reaction occurring during the synthesis procedure. The peak at approximately 508 cm^{-1} in the S@TE7 spectra implies disulfide stretching modes for a variety of alkyl, allyl and aryl disulfides. All materials were ground prior to data acquisition. SWCNT data was not collected owing to nanomaterial safety concerns.

Repeat Gravimetric Hydrogen Sorption Measurement

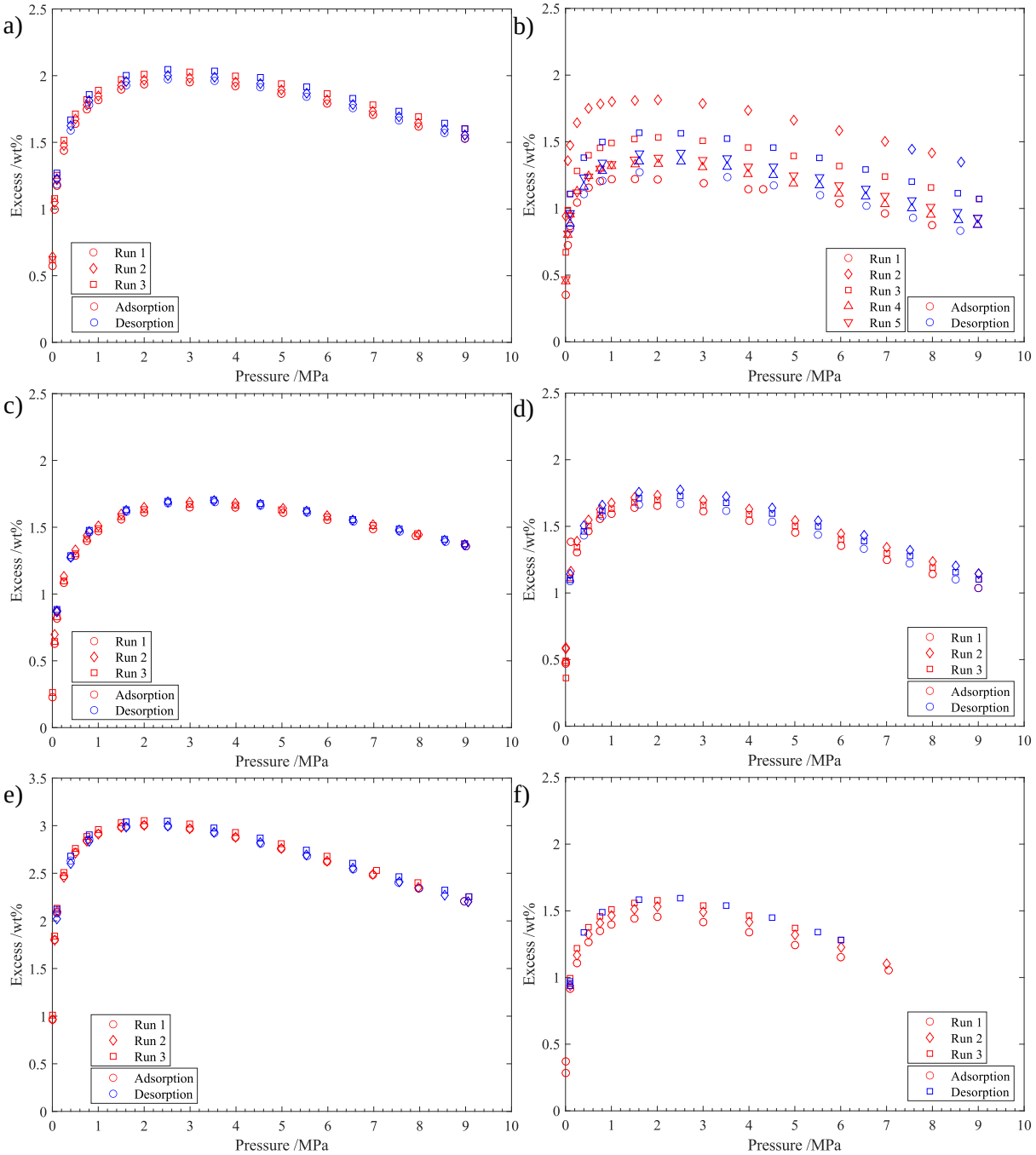

Figure S8: Repeat 77 K H_2 sorption measurements for a) for w-SWCNT-121; b) S@SWCNT-12;. C) w-SWCNT-777; d) S@SWCNT-777. E) w-TE7. F) S@TE7. For all plots red denotes adsorption, blue denotes desorption.

Literature Comparison of Sulfur-Doped Porous Carbons

Table S3: Comparison of maximum empirically determined hydrogen uptakes at 77 K for different porous carbon/sulfur composite materials reported in literature.

Author	Sample	Specific Surface Area /$m^2.g^{-1}$	N_e^{max} H_2 /wt%	Pressure /MPa	Temperature /K	Reference
This report	w-SWCNT-121 [a]	869	1.99	9	77	-
This report	S@SWCNT-121	752	1.35	9	77	-
This report	w-SWCNT-777 [a]	1011	1.67	9	77	-
This report	S@SWCNT-777	764	1.70	9	77	-
This report	S2@SWCNT-777	437	0.66	9	77	-
This report	w-TE7 [a]	1200	3.02	9	77	-
This report	S@TE7	1008	1.52	7 [b]	77	-
Xia *et al.*	SCEMC	729	3	2	77	[17]
Xia *et al.*	SCEMC600	803	2.11	2	77	[17]
Xia *et al.*	SCEMC700	1627	4.43	2	77	[17]
Xia *et al.*	SCEMC800	1035	2.96	2	77	[17]
Xia *et al.*	CEMC [a]	1658	3.86	2	77	[17]
Zheng *et al.*	SCMS	432.2	3.3	0.9	77	[14]
Zheng *et al.*	CMS [a]	15.5	0.98	0.9	77	[14]
Sevilla *et al.*	ACT-600	1790	4.55	2	77	[18]
Sevilla *et al.*	ACT-700	1980	4.8	2	77	[18]
Sevilla *et al.*	ACT-750	2810	5.19	2	77	[18]
Sevilla *et al.*	ACT-800	3010	5.4	2	77	[18]
Sevilla *et al.*	ACT-850	3000	5.71	2	77	[18]
Li *et al.*	TC [a]	1236	2.24	0.4	77	[19]
Li *et al.*	S1	755	1.87	0.4	77	[19]
Li *et al.*	S2	962	2.61	0.4	77	[19]
Li *et al.*	S3	943	2.72	0.4	77	[19]
Wang *et al.*	CU-800 [a]	874	1.75 [c]	0.1	77	[20]
Wang *et al.*	CT-800	1260	2.38	0.1	77	[20]
Park et al.	AC	885	1.51	2	77	[21]
Park *et al.*	GL	310	0.67	2	77	[21]

[a] *Comparative material without sulfur.*

[b] *Inlet pressure failed to reach 9 MPa due to depletion of the gas cylinder.*

[c] *estimated by converting the reported volumetric value to a mass of hydrogen (molar volume = 22.4 $dm^3.g^{-1}$ at STP)*

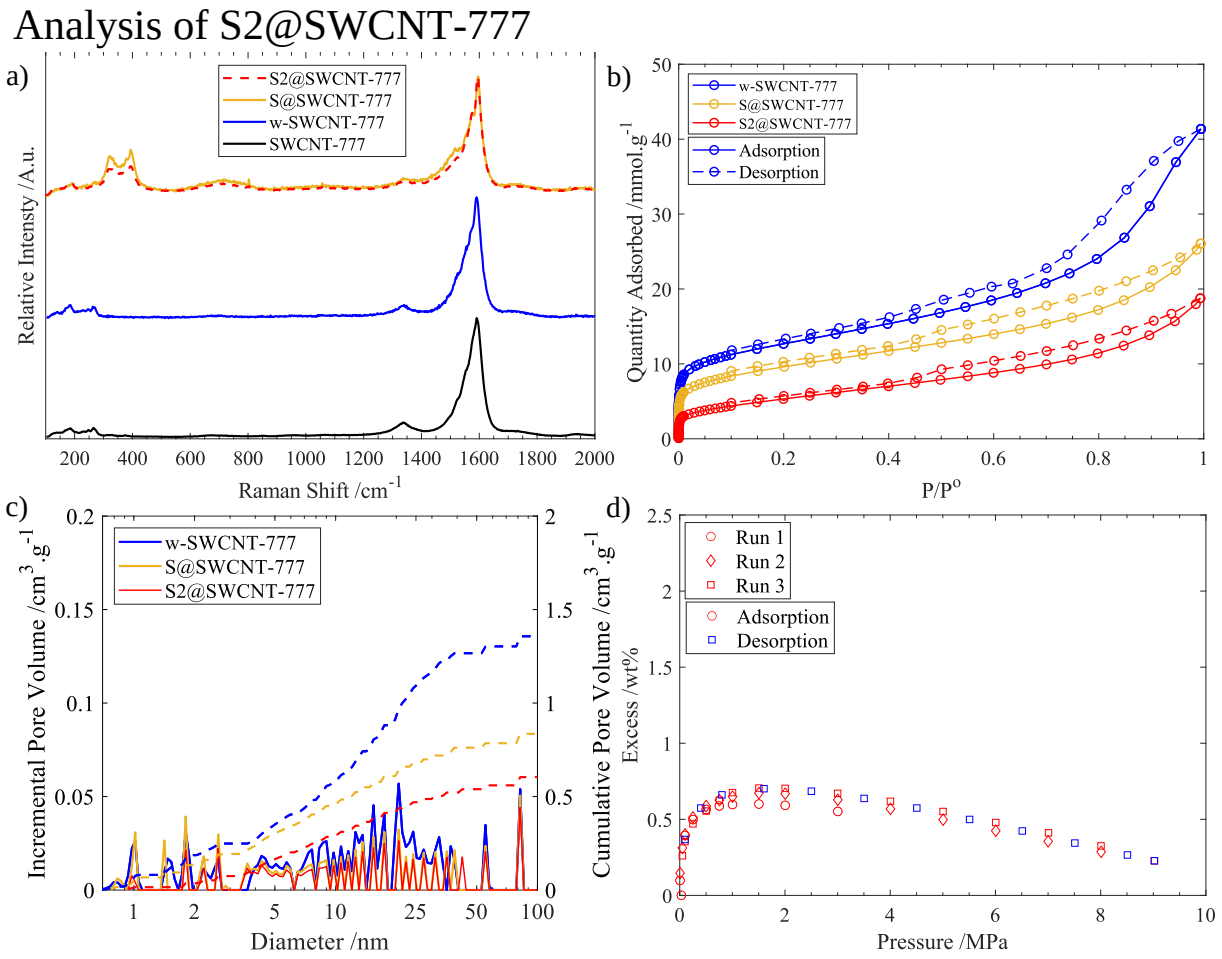

Figure S9: a) Raman spectra for SWCNT-777 (black), w-SWCNT-777 (blue), S@SWCNT-777 (yellow), S2@SWCNT-777 (red dashed) at 532 nm excitation wavelength. Radial breathing mode (100-350 cm^{-1}) and polysulfide modes at 320 cm^{-1} and 395 cm^{-1} are present and bare resemblance to S@SWNCT-777. b) 77 K N_2 sorption isotherms for w-SWCNT-777 (blue), S@SWCNT-777 (yellow) and S2@SWCNT-777 (red). BET specific surface area for S2@SWCNT-777 is 435±2 $m^2.g^{-1}$, total V_p is 0.55 $cm^{-3}.g^{-1}$ and Dubinin-Radushkevich μV_p is 0.16 $cm^3.g^{-1}$. c) Incremental and cumulative pore volume for w-SWCNT-777 (blue), S@SWCNT-777 (yellow) and S2@SWCNT-777 (red) determined via NLDFT using cylindrical pore model. d) Triplicate 77 K H_2 gravimetric isotherms for S2@SWCNT-777 adsorption (red), desorption (blue).

Fitting Parameters for Semi-Empirical Modelling of All H_2 sorption Isotherms

Table S4: Summary of values determined through fitting of equation 1 (see main manuscript text) of the H_2 isotherms and the goodness of fit values for each fitting.

Sample	Run no.	ρ_a /g.cm^{-3}		b /MPa^{-1}		c / Unitless		V_p /cm^3.g^{-1}	χ^2	r^2
		Value	σ^2	Value	σ^2	Value	σ^2			
w-SWCNT-121	1	0.06714	9.52E-04	103537.073	38295.29193	0.13416	0.00306	1.19	3.05E-04	0.99796
	2	0.06893	1.31E-03	370011.0846	198044.29	0.12579	0.00379	1.19	5.22E-04	0.99632
	3	0.07109	1.84E-03	814785.9322	610967.7498	0.12099	0.00485	1.19	9.32E-04	0.9939
S@SWCNT-121	1	0.05179	1.38E-03	347266.1476	375085.6733	0.13035	0.00763	0.94	0.00124	0.98041
	2	0.06676	9.40E-04	4.55E+10	4.25E+10	0.08904	0.00262	0.94	3.27E-04	0.99492
	3	0.06066	3.32E-04	4.15E+07	1.03E+07	0.10823	0.00114	0.94	3.65E-05	0.99936
	4	0.05263	8.61E-04	7.67E+05	4.98E+05	0.1282	0.00442	0.94	4.01E-04	0.9933
	5	0.05562	2.68E-04	757394.4231	135775.7256	0.12663	0.00121	0.94	3.07E-05	0.99951
w-SWCNT-777	1	0.06375	9.35E-04	1199.3169	313.54072	0.16356	0.00373	1.28	2.53E-04	0.99851
	2	0.06491	4.73E-04	3429.10149	494.80109	0.15286	0.00174	1.28	5.60E-05	0.99944
	3	0.06421	8.38E-04	1285.0991	297.18367	0.163	0.00327	1.28	2.02E-04	0.9988
S@SWCNT-777	1	0.05241	1.89E-03	13758.07617	13942.94832	0.1842	0.01513	0.78	4.06E-03	0.97056
	2	0.05585	4.44E-04	16153.86902	3451.21887	0.17952	0.00306	0.78	1.74E-04	0.99869
	3	0.05231	1.44E-03	1278.43853	780.85342	0.22052	0.01413	0.78	2.61E-03	0.98377
S2@SWCNT-777	1	0.02269	3.88E-03	9.08956	9.07289	0.516	0.20863	0.55	0.0056	0.88495
	2	0.03555	2.46E-04	510.13631	95.18913	0.22167	0.00438	0.55	4.63E-05	0.99823
	3	0.03589	6.23E-04	29.17749	10.44484	0.30551	0.01801	0.55	5.22E-04	0.98729
w-TE7	1	0.07195	8.73E-04	2461.72486	685.23421	0.25975	0.0086	0.68	0.00109	0.9963
	2	0.07217	8.29E-04	2271.48762	592.3363	0.26055	0.00814	0.68	9.64E-04	0.9967
	3	0.07335	8.73E-04	2880.3436	793.29906	0.25539	0.0082	0.68	0.00103	0.9965
S@TE7	1	0.04774	8.50E-04	549.05163	163.77376	0.24143	0.00892	0.71	5.07E-04	0.99638
	2	0.04895	3.94E-03	583.474	1116.4431	0.24259	0.05361	0.71	0.00646	0.96805
	3	0.0511	8.02E-03	1219.08147	4231.40489	0.22575	0.08471	0.71	0.01357	0.93572

References

1. Lemmon, E.W., et al., Thermophysical Properties of Fluid Systems, in NIST Chemistry WebBook, NIST Standard Reference Database Number 69, P.J. Linstom and W.G. Mallard, Editors., National Institute of Standards and Technology Gaithersburg MD. (accessed August 24 2022)
2. Carbon X-ray photoelectron spectra, carbon electron configuration, and other elemental information, https://www.thermofisher.com/uk/en/home/materials-science/learning-center/periodic-table/non-metal/carbon.html, (accessed 08/12/2022, 2022).
3. L. Leng, R. Liu, S. Xu, B. A. Mohamed, Z. Yang, Y. Hu, J. Chen, S. Zhao, Z. Wu and H. Peng, *Journal of Environmental Chemical Engineering*, 2022, 107185.
4. M. Fantauzzi, B. Elsener, D. Atzei, A. Rigoldi and A. Rossi, *RSC Advances*, 2015, **5**, 75953-75963.
5. C.-P. Yang, Y.-X. Yin, Y.-G. Guo and L.-J. Wan, *Journal of the American Chemical Society*, 2015, **137**, 2215-2218.
6. Sulfur X-ray photoelectron spectra, sulfur electron configuration, and other elemental information, https://www.thermofisher.com/uk/en/home/materials-science/learning-center/periodic-table/non-metal/sulfur.html, (accessed 08/12/2022, 2022).
7. X-ray Photoelectron Spectroscopy (XPS) Reference Pages, http://www.xpsfitting.com/search/label/Sulphur, (accessed 08/12/2022, 2022).
8. U. Zubair, J. Amici, S. M. Crespiera, C. Francia and S. Bodoardo, *Carbon*, 2019, **145**, 100-111.
9. S. Huang, Q. Liang, J. Geng, H. Luo and Q. Wei, *Mater. Chem. Phys.*, 2019, **238**, 121919.
10. L. Qie, W. Chen, X. Xiong, C. Hu, F. Zou, P. Hu and Y. Huang, *Advanced Science*, 2015, **2**.
11. T. Fujimori, A. Morelos-Gómez, Z. Zhu, H. Muramatsu, R. Futamura, K. Urita, M. Terrones, T. Hayashi, M. Endo and S. Y. Hong, *Nature Communications*, 2013, **4**, 1-8.
12. H. Li, W. Zhu, J. Yang, M. Zhang, J. Zhao and W. Qu, *Fuel*, 2018, **232**, 476-484.
13. J. Mycroft, G. Bancroft, N. McIntyre, J. Lorimer and I. Hill, *Journal of Electroanalytical Chemistry and Interfacial Electrochemistry*, 1990, **292**, 139-152.
14. M. Zheng, H. Zhang, Y. Xiao, H. Dong, Y. Liu, R. Xu, Y. Hu, B. Deng, B. Lei and X. Liu, *Mater. Lett.*, 2013, **109**, 279-282.
15. A. M. de Yuso, M. De Fina, C. Nita, P. Fioux, J. Parmentier and C. M. Ghimbeu, *Microporous and Mesoporous Materials*, 2017, **243**, 135-146.
16. T. R. Gengenbach, G. H. Major, M. R. Linford and C. D. Easton, *Journal of Vacuum Science & Technology A: Vacuum, Surfaces, and Films*, 2021, **39**, 013204.
17. Y. Xia, Y. Zhu and Y. Tang, *Carbon*, 2012, **50**, 5543-5553.
18. M. Sevilla, A. Fuertes and R. Mokaya, *International Journal of Hydrogen Energy*, 2011, **36**, 15658-15663.
19. D. Li, W. Li, J. Shi and F. Xin, *RSC Advances*, 2016, **6**, 50138-50143.

20. D. Wang, Y. Shen, Y. Chen, L. Liu and Y. Zhao, *Chem. Eng. J.*, 2019, **367**, 260-268.

21. J. Park, N. F. Attia, M. Jung, M. E. Lee, K. Lee, J. Chung and H. Oh, *Energy*, 2018, **158**, 9-16